Int. J. Solids Structures, 1976, Vol. 12, pp. 419–429. Pergamon Press. Printed in Great Britain.

PULSE PROPAGATION IN BOUNDED HELICAL COIL ASSEMBLIES

NAGYOUNG CHANG† and DANIEL W. HAINES
College of Engineering, University of South Carolina, Columbia, SC 29208, U.S.A.

(*Received* 21 *August* 1975; *revised* 7 *November* 1975)

Abstract—The problem of an extensional stress pulse applied to a bounded helical coil assembly is formulated and solved. The assembly is composed of one turn of a small pitched coil attached tangentially to two straight segments. One end of the assembly is always fixed while the other is free when not subjected to the action of the pulse. It is found that to prevent significant portions of the shock from reaching the fixed end, the pulse length should be longer than the circumference of the coil but shorter than twice the length of the initial straight segment. Flexural energy continuously leaks into the coil from the straight segment. Experiments were performed which verify the analytical solution.

INTRODUCTION

The propagation of elastic tangential stress pulses along helical coils and curved bars has been studied by a number of investigators[1–6]. This paper extends the work of [6] to a bounded helical coil assembly. We also establish design criteria for the use of such an assembly as a shock absorber.

Our helical coil assembly consists of three segments; two straight segments and one helical coil segment, all made of the same material and with identical cross-sections. They are joined tangentially as shown in Fig. 1 with one end fixed. The assembly is at rest until a tangential stress pulse is applied to the otherwise free end of the assembly. The subsequent behavior of the assembly is studied analytically and verification is provided by experiment. The design criteria are drawn from these results.

As in previous paper[6], the two mode theory of coupled extension and flexure is used as the governing theory for the helical coil, and the classical extensional theory of bars and the Bernoulli-Euler beam theory is used for straight segments. These theories are valid in the frequency range from zero to at least 1/15 of the thickness-shear cut-off frequency[7]. The duration of the pulse considered is on the order of the period of the ring mode vibration of the helical coil, and therefore the pulse has only a small portion of frequency components above the frequency range of validity of theories employed[7].

The analytical solution is obtained by use of the Fourier time transform and the complex frequency response of the assembly. Since the helical coil assembly is a bounded, distributed mechanical system, it has an infinite number of eigenfrequencies. These eigenfrequencies are simple poles of the complex frequency response. Since the assembly is assumed to be elastic and thus a conservative mechanical system, all the eigenfrequencies are real. Hence, the Fourier inversion integral is evaluated through residue calculation. As a result, the integral solution is transformed into a series solution, each term in the series representing an eigenmode. For most considerations the eigenmodes corresponding to essentially extensional motion dominate as can be anticipated from the nature of the applied pulse.

The numerical results agree well with the experiments. It is observed that the frequency components below the ring mode frequency are largely captured in the initial straight segment, whereas those components above the ring mode frequency travel back and forth along the helical coil assembly. The low frequency components are seen to be transformed into flexural waves gradually. These low frequency flexural waves then propagate along the helical coil assembly with a group velocity much lower than the bar velocity.

The use of the assembly as a shock absorber employs its ability to trap energy in the straight

†Present address: Department of Civil Engineering, Princeton University, Princeton, NJ 08540, U.S.A.

section. Continuous leakage of flexural energy diminishes the assembly's usefulness in this application.

ANALYTICAL SOLUTION

The governing equations of motion and the constitutive equations are written in non-dimensional form as in the previous paper [6]. Thus, the equations of motion for a helical coil of small pitch:

$$\begin{aligned} -ku'''' - u + kv''' - v' &= \ddot{u}, \\ -ku''' + u' + (1+k)v'' &= \ddot{v}, \end{aligned} \tag{1}$$

the constitutive equations for a helical coil of small pitch:

$$\begin{aligned} \psi &= v - u', \\ P &= v' + u, \\ Q &= k(v'' - u'''), \\ M &= k(v' - u''), \end{aligned} \tag{2}$$

the equations of motion for the straight segments:

$$\begin{aligned} -ku'''' &= \ddot{u}, \\ v'' &= \ddot{v}, \end{aligned} \tag{3}$$

and the constitutive equations for the straight segments:

$$\begin{aligned} \psi &= -u', \\ P &= v', \\ Q &= -ku''', \\ M &= -ku''. \end{aligned} \tag{4}$$

All symbols in (1)–(4) are non-dimensional, where u and v are lateral and tangential displacements, ψ is the rotation, P and Q are tangential and shear forces, and M is the bending moment. Prime and dot represent the partial differentiation with respect to the non-dimensional spatial variable, θ, and the non-dimensional time, τ, respectively. The geometric constant k is defined to be I/AR^2 and the bar velocity c is $(E/\rho)^{1/2}$, where I is the second moment of area of the cross section of the assembly, A is the cross-sectional area, R is the mean radius of the helical coil, E is the Young's modulus and ρ is the density of the material. In general, the scheme of the non-dimensionalization is such that the length-like quantities are divided by R, the velocity-like quantities are divided by c, and the force-like quantities are divided by EA.

The boundary conditions are as shown in Fig. 1, except that the end, $\theta = \theta_1$, receives the tangential stress pulse starting at $\tau = 0$. Thus, the boundary conditions are

$$\begin{aligned} &P(\theta_1, \tau) = h(\tau), \\ &Q(\theta_1, \tau) = 0, \\ &M(\theta_1, \tau) = 0, \\ &\Phi(\theta_{2^-}, \tau) = \Phi(\theta_{2^+}, \tau), \quad \text{for} \quad \Phi \epsilon [u, v, \psi, P, Q, M], \\ &\Phi(\theta_{3^-}, \tau) = \Phi(\theta_{3^+}, \tau), \quad \text{for} \quad \Phi \epsilon [u, v, \psi, P, Q, M], \\ &u(\theta_4, \tau) = v(\theta_4, \tau) = \psi(\theta_4, \tau) = 0 \\ &\text{for all } \tau. \end{aligned} \tag{5}$$

The input function, $h(\tau)$, satisfies the condition

$$h(\tau) = 0, \quad \text{for all } \tau < 0. \tag{6}$$

The initial conditions call for the assembly to be quiescent until $\tau = 0$. Thus,

$$u(\theta, \tau) = v(\theta, \tau) = 0,$$
$$\text{for } \theta_1 \leq \theta \leq \theta_4, \quad \text{for all } \tau < 0. \tag{7}$$

The solution is obtained by introducing the Fourier time transforms and the complex frequency responses. The Fourier transforms are defined by

$$\bar{h}(\Omega) = \int_{-\infty}^{\infty} h(\tau) \exp(-i\Omega\tau)\, d\tau,$$
$$\bar{\Phi}(\theta, \Omega) = \int_{-\infty}^{\infty} \Phi(\theta, \tau) \exp(-i\Omega\tau)\, d\tau, \tag{8}$$
$$\text{for } \Phi \epsilon [u, v, \psi, P, Q, M],$$

and the complex frequency responses are[5]

$$G_\Phi(\theta, \Omega) = \bar{\Phi}(\theta, \Omega)/\bar{h}(\Omega),$$
$$\text{for } \Phi \epsilon [u, v, \psi, P, Q, M]. \tag{9}$$

The expressions for complex frequency responses are obtained by considering the solution which varies sinusoidally in time and which satisfies the boundary conditions of (5) with $h(\tau) = \exp(i\Omega\tau)$. Thus, if $P(\theta_1, \tau) = \exp(i\Omega\tau)$, then $\Phi = G_\Phi(\theta, \Omega) \exp(i\Omega\tau)$[5].

Such a solution may be obtained as a superposition of all the harmonic wave solutions with frequency Ω. Let us take

$$u = a \exp[i(\Omega\tau - Z\theta)],$$
$$v = b \exp[i(\Omega\tau - Z\theta)], \tag{10}$$

as the harmonic wave solution of the equation of motion. By substituting (10) into the equations of motion (1) and (3), we get the frequency equations. Thus, for straight segments we obtain

$$kZ^4 - \Omega^2 = 0,$$
$$Z^2 - \Omega^2 = 0, \tag{11}$$

for the flexural motion and the extensional motion respectively, and for helical coil segments we get

$$kZ^6 - k(\Omega^2 + 2)Z^4 + [-(1 + k)\Omega^2 + k]Z^2 + \Omega^2(\Omega^2 - 1) = 0. \tag{12}$$

The flexural motion and the extensional motion are uncoupled in the straight segments. However, they are coupled in the helical coil segments, as is apparent from the equations of motion for helical coil. Hence, for the helical coil segment the amplitudes, a and b of (10), are related by the amplitude ratio r which depends upon Ω and Z;

$$b = ar,$$
$$r = [iZ - k(iZ)^3]/[\Omega^2 + (1 + k)(iZ)^2]. \tag{13}$$

By superimposing all the harmonic wave solutions with frequency Ω for each segment of the assembly, we get the general solution which varies sinusoidally in time with frequency Ω. Thus,

for the straight segment P_1P_2 we have

$$\begin{aligned} u &= \sum_{j=1}^{4} a_j \exp[i(\Omega\tau - Z_j\theta)], \quad \theta_1 \le \theta \le \theta_2, \\ v &= \sum_{j=5}^{6} a_j \exp[i(\Omega\tau - Z_j\theta)], \quad \theta_1 \le \theta \le \theta_2, \end{aligned} \tag{14}$$

and for the helical coil segment P_2P_3 we have

$$\begin{aligned} u &= \sum_{j=7}^{12} a_j \exp[i(\Omega\tau - Z_j\theta)], \quad \theta_2 \le \theta \le \theta_3, \\ v &= \sum_{j=7}^{12} a_j r_j \exp[i(\Omega\tau - Z_j\theta)], \quad \theta_2 \le \theta \le \theta_3, \end{aligned} \tag{15}$$

and for the straight segment P_3P_4:

$$\begin{aligned} u &= \sum_{j=13}^{16} a_j \exp[i(\Omega\tau - Z_j\theta)], \quad \theta_3 \le \theta \le \theta_4, \\ v &= \sum_{j=17}^{18} a_j \exp[i(\Omega\tau - Z_j\theta)], \quad \theta_3 \le \theta \le \theta_4. \end{aligned} \tag{16}$$

The wave numbers $Z_1 \ldots Z_4$ are the roots of (11a); the wave numbers Z_5, Z_6 are the roots of (11b); the wave numbers $Z_7 \ldots Z_{12}$ are the roots of (12); the wave numbers $Z_{13} \ldots Z_{16}$ are the roots of (11a) again, and the wave numbers Z_{17}, Z_{18} are the roots of (11b) again. The amplitude ratios $r_7 \ldots r_{12}$ are obtained by substituting $Z_7 \ldots Z_{12}$ into (13), respectively. Equations (14)–(16) represent the general solution which varies sinusiodally with frequency Ω. Other quantities such as ψ, P, Q and M can be obtained by substituting these equations into the proper constitutive equations (either (2) or (4) depending on the type of segment).

There are eighteen constants in (14)–(16), namely $a_1 \ldots a_{18}$. These constants will be determined uniquely if we impose the boundary condition of (5) with $h(\tau)$ replaced by $\exp(i\Omega\tau)$ in (5a). The boundary conditions lead to the matrix equation

$$[U][a] = [e], \tag{17}$$

where

$$\begin{aligned} [a] &= [a_1 \quad \ldots \quad a_{18}]^T, \\ [e] &= [1 \quad 0 \quad 0 \quad \ldots \quad 0]^T, \end{aligned} \tag{18}$$

T denoting the transpose of the matrix.
The solution of (17) is $[a] = [U]^{-1}[e]$, or in subscript notation,

$$a_j = U_{j1}^{-1}, \quad \text{for all } j. \tag{19}$$

Substitution of this into (14)–(16) yields the sinusoidally varying solution that satisfies the boundary conditions of (5) with $h(\tau) = \exp(i\Omega\tau)$. Also, the use of constitutive equations (either (2) or (4) depending on the type of segment) produces ψ, P, Q and M. Recalling that for harmonic excitation we have $\Phi = G_\Phi(\theta, \Omega)\exp(i\Omega\tau)$, we then obtain the explicit expressions for complex frequency responses for which we show only $G_p(\theta, \Omega)$:

$$G_p(\theta, \Omega) = \begin{cases} \sum_{j=5}^{6} - U_{j1}^{-1} iZ_j \exp(-iZ_j\theta), & \theta_1 \le \theta \le \theta_2, \\ \sum_{j=7}^{12} U_{j1}^{-1}(1 - iZ_j r_j)\exp(-iZ_j\theta), & \theta_2 \le \theta \le \theta_3, \\ \sum_{j=17}^{18} - U_{j1}^{-1} iZ_j \exp(-iZ_j\theta), & \theta_3 \le \theta \le \theta_4. \end{cases} \tag{20}$$

The complex frequency responses for $\Omega = 0$ are of particular interest. For $\Omega = 0$ the problem degenerates into the static problem, and therefore $G_\Phi(\theta, 0)$ represents the static solution which satisfies the boundary conditions of (5) with $h(\tau) = 1$ in (5a).

It is to be observed that $G_\Phi(\theta, \Omega)$ is not defined if the system matrix, $[U]$, is singular which occurs at resonance frequencies of the system for $h(\tau) = 0$, i.e., eigenfrequencies. The following statements concerning the eigenfrequency have been proved in [8] for this particular helical coil assembly, and these statements are valid for any finite, continuous, one-dimensional, non-dissipative mechanical systems in general; (1) There are infinitely many eigenfrequencies for the system. (2) The eigenfrequencies are real. (3) Eigenfrequencies are simple poles of $[U]^{-1}$, and hence of $G_\Phi(\theta, \Omega)$. (4) Eigenfrequencies are the only poles of $G_\Phi(\theta, \Omega)$. (5) If Ω_n is an eigenfrequency, Res $G_\Phi(\theta, \Omega_n)$ is real, and

$$\text{Res } G_\Phi(\theta, -\Omega_n) = -\text{Res } G_\Phi(\theta, \Omega_n).$$

The solution that satisfies the boundary conditions and the initial conditions of (5)–(7) can be obtained from (8) and (9) as a Fourier integral;

$$\Phi(\theta, \tau) = \frac{1}{2\pi} \int_C G_\Phi(\theta, \Omega) \bar{h}(\Omega) \exp(i\Omega\tau)\, d\Omega, \tag{21}$$

where C is the contour of integration that extends from $\Omega = -\infty$ to $\Omega = \infty$, but always below the real-Ω-axis. We choose this contour instead of the real-Ω-axis to by-pass the eigenfrequencies, which are poles of $G_\Phi(\theta, \Omega)$. Also, by use of Jordan's lemma and the residue theory [9] the integral of (21) proves to be zero for $\tau < 0$, which is in accordance with the initial conditions of (7). Now suppose that the input pulse is a rectangular pulse with unit magnitude and duration τ_0. Then,

$$h(\tau) = H(\tau) H(\tau_0 - \tau), \tag{22}$$

where H represents the Heaviside unit step function. From (8) and (22) we get

$$\bar{h}(\Omega) = [1 - \exp(-i\Omega\tau_0)]/i\Omega. \tag{23}$$

Substitution of this into (21) and the use of Jordan's lemma and the residue theory lead to a series solution

$$\Phi(\theta, \tau) = \begin{cases} G_\Phi(\theta, 0) + 2 \sum_{n=1}^{\infty} \text{Re}[i\bar{H}(\Omega_n) \exp(i\Omega_n\tau)] \text{ Res } G_\Phi(\theta, \Omega_n), & \tau \geq \tau_0, \\ 2 \sum_{n=1}^{\infty} \text{Re}[i\bar{h}(\Omega_n) \exp(i\Omega_n\tau)] \text{ Res } G_\Phi(\theta, \Omega_n), & \tau \geq \tau_0, \end{cases} \tag{24}$$

where $\bar{H}(\Omega) = 1/i\Omega$, and Ω_1, $\Omega_2 \ldots$ are eigenfrequencies. For more detailed discussion concerning the derivation of the series type solution the reader is referred to Ref. [8].

Since the eigenfrequencies are the simple poles of $[U]^{-1}$, it is apparent from (20) that Res $G_\Phi(\theta, \Omega_n)$ can be expressed as a linear combination of Res $U_{j1}^{-1}(\Omega_n)$. Thus,

$$\text{Res } G_p(\theta, \Omega_n) = \begin{cases} \sum_{j=5}^{6} -iZ_{nj} \exp(-iZ_{nj}\theta) \text{ Res } U_{j1}^{-1}(\Omega_n), & \theta_1 \leq \theta \leq \theta_2, \\ \sum_{j=7}^{12} (1 - iZ_{nj}r_{nj}) \exp(-iZ_{nj}\theta) \text{ Res } U_{j1}^{-1}(\Omega_n), & \theta_2 \leq \theta \leq \theta_3, \\ \sum_{j=17}^{18} -iZ_{nj} \exp(-iZ_{nj}\theta) \text{ Res } U_{j1}^{-1}(\Omega_n), & \theta_3 \leq \theta \leq \theta_4, \end{cases} \tag{25}$$

where

$$\begin{aligned} Z_{nj} &= Z_j]_{\Omega=\Omega_n}, \qquad j = 1 \ldots 18, \qquad n = 1, 2 \ldots, \\ r_{nj} &= r_j]_{\Omega=\Omega_n}, \qquad j = 7, 8 \ldots 12, \quad n = 1, 2 \ldots, \end{aligned} \tag{26}$$

and other residues follow this example. Note that for each term in the series of (24) the time dependence is a harmonic function of frequency Ω_n. Thus, each term represents the contribution to the response of one resonance with magnitude given by the product of Res $G_\Phi(\theta, \Omega_n)$, a system property, and $\bar{h}(\Omega_n)$ known from the input Fourier spectrum. The Res $G_\Phi(\theta, \Omega_n)$ will be large if the mode of free vibration corresponding to Ω_n tends to be excited by the pulse, e.g. an essentially extensional mode is strongly excited by a tangential pulse, an essentially flexural mode is not.

NUMERICAL RESULT

For the numerical calculation, we assumed the following data;

$$k = 7.56 \times 10^{-4},$$
$$\theta_2 - \theta_1 = 4,\ \theta_3 - \theta_2 = 2\pi,\quad \theta_4 - \theta_3 = 4, \tag{27}$$
$$\tau_0 = 2\pi.$$

The computation of the solution consists of four steps. As a first step, the eigenfrequencies were found and refined. This was done by computing the determinant of the system matrix $[U]$. Since the eigenfrequencies are known to be on the real frequency axis, a bisection method was devised to refine the value of every eigenfrequency. The second step was to compute

$$\text{Res } U_{j1}^{-1}(\Omega_n),\quad j = 1, 2 \ldots 18,\quad n = 1, 2 \ldots .$$

This was done by the following approximate equation for the residue as calculated from a closed contour of radius r encircling Ω_n.

$$\text{Res } U_{j1}^{-1}(\Omega_n) \simeq \frac{r}{N} \sum_{m=1}^{N} \exp(2\pi m i/N)\, U^{-1}[\Omega_n + r \exp(2\pi m i/N)]. \tag{28}$$

Theoretically, this approximate equation becomes exact as $r \to 0$ and $N \to \infty$. For practical purpose, we used $N = 30$ and various values of r ranging from $10^{-10}\,\Omega_n$ to $10^{-7}\,\Omega_n$. The third step was to compute Res $G_\Phi(\theta, \Omega_n)$. This was done by (25) and analogous equations for Res $G_Q(\theta, \Omega_n)$ and Res $G_M(\theta, \Omega_n)$. Finally, $P(\theta, \tau)$, $Q(\theta, \tau)$ and $M(\theta, \tau)$ were obtained from (24) and (23). The series of (24) was truncated at the 65-th term. The numerical calculation shows that $\Omega_{65} = 3.261$, and therefore the series after truncation accounts for frequency components up to $\Omega_{\max} = 3.261$. Since τ_0 is assumed to be 2π, the third zero of the input frequency spectrum, $|\bar{h}(\Omega)|$, falls at $\Omega = 3$. Thus we can expect that the truncated portion would be insignificant. Also, the two mode theory begins to diverge from the exact theory above this frequency, and therefore truncation at $\Omega_{\max} = 3.261$ appears to be reasonable. The calculation was performed on an IBM/370 computer using complex, double precision variables.

The numerical results were plotted in Figs. 3–10 as solid lines. Figure 3 is the shape of the input tangential stress pulse. It is not strictly rectangular, because we truncated the frequency components above $\Omega_{\max}$. Figure 4 represents the tangential stress at the mid-point of the straight segment P_1P_2. The first wave in this figure represents the passing of the input rectangular pulse. The subsequent waves indicate that a large portion of input pulse is captured in the straight segment P_1P_2. The captured wave travels back and forth in the straight segment, being inverted every time it is reflected. The dominant frequency of the captured wave is about $\Omega = 0.608$, which is lower than the ring mode frequency ($\Omega = 1$). Figure 5 represents the stress at point P_2, the junction between the first straight segment and the helical coil segment. The first wave in this figure represents the arrival of the input pulse. As in Fig. 4, an inverted reflected wave appears also. There is a time lag between the arrival of the input pulse and the arrival of the reflected wave at point P_2. This suggests that the input pulse continues to pass at least a short distance into the helical coil segment, where it undergoes a gradual reflection because of the continuous change in the direction of propagation. Figure 6 represents the stress at point P_3. The peak of the first significant ripple arrives roughly with the bar velocity, and the dominant frequency of this ripple

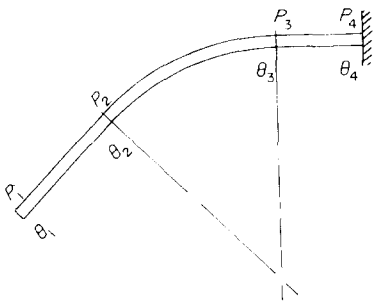

Fig. 1. Helical coil assembly.

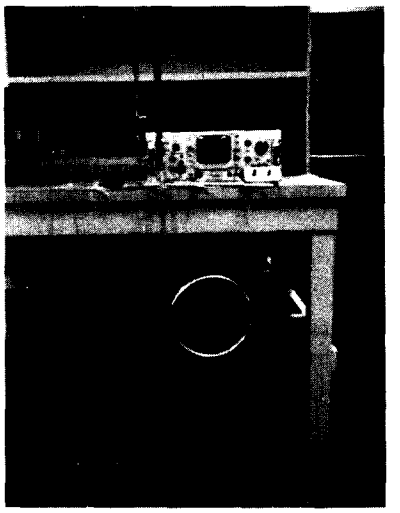

Fig. 2. Experimental setup.

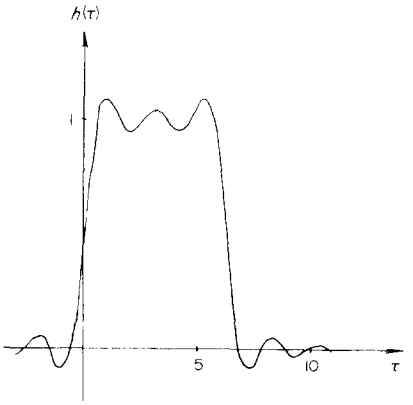

Fig. 3. Input tangential stress pulse.

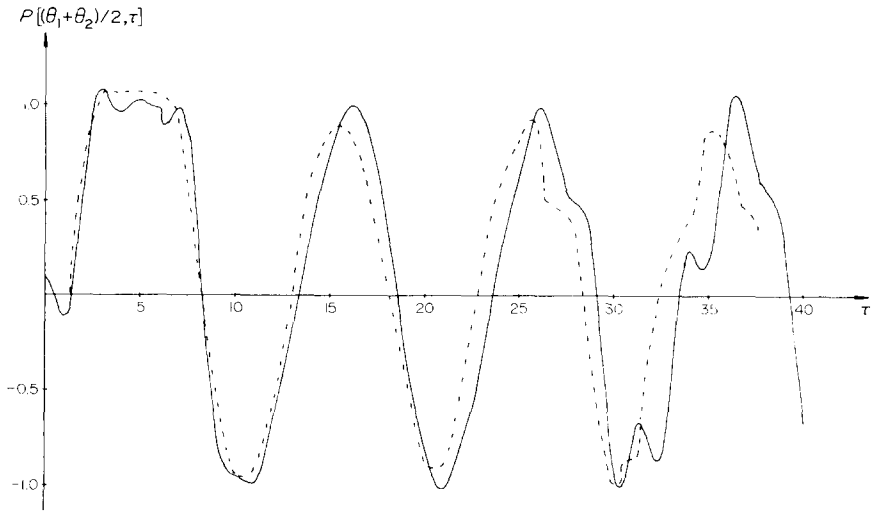

Fig. 4. Tangential stress at the mid-point of P_1P_2 (dotted line represents experimental result).

is about $\Omega = 2.42$. Thus, from the nature of the input pulse, it is not surprising that the first signal to reach a point within the coil is associated with the portion of the extensional branch with highest group velocity. The frequency of the subsequent ripples is lower than this but still higher than the ring mode frequency ($\Omega = 1$) as expected. Figure 7 represents the extensional stress at point P_4, the fixed end of the assembly. The magnitude of the first few ripples in this figure is twice that of the first few ripples in Fig. 6 because the ripples are being reflected at this fixed end. Returning to Figs. 4 and 5, we now recognize that the high frequency components which we observe for $25 \leq \tau \leq 40$ are the ripples which returned from a round trip to the fixed end, P_4.

Thus, it is observed that the frequency components below the ring mode frequency are largely captured in the initial straight segment, whereas the frequency components above it are travelling along the whole assembly.

By assuming that the cross-section of the assembly is circular, the outside and the inside fiber stresses can be shown to be[8]

$$P_{\pm} = P \pm 2k^{-1/2}M. \tag{29}$$

From this equation, the outside and inside fiber stresses were computed and then plotted on Figs. 8 and 9, respectively. It is immediately apparent that the flexural stress is almost solely responsible for the growth of the stress at the fixed end. Also, it is to be noted that there appear to be two dominant frequency components. The most pronounced frequency component is $\Omega = 0.63$, which is close to the frequency of the captured wave. This suggests that some flexural waves leak into the coil every time the captured waves return to the junction area. Superimposed with those are very low frequency components. The dominant frequency of these is about $\Omega = 0.01$ at first, but it is even lower as time passes. These can be identified as waves of low group velocity contributed by the very low frequency portion of the dispersion curves of the coil where three branches are real[7]. Figure 10 shows the portions of the total input energy which were transmitted beyond points P_2 and P_3 as functions of τ. This was obtained by use of the following equations:

$$\begin{aligned} E_I &= \int_{-\infty}^{\infty} [-P\dot{v} - Q\dot{u} - M\dot{\psi}]_{\theta=\theta_1}\, d\tau, \\ E_j &= \int_{-\infty}^{\tau} [-P\dot{v} - Q\dot{u} - M\dot{\psi}]_{\theta=\theta_j}\, d\tau, \quad j = 2, 3, \end{aligned} \tag{30}$$

where E_I is the total input energy, and E_j is the energy that was transmitted beyond the point P_j. Due to the dispersion of the helical coil and trapping of energy in the initial straight segment, the energy flow rate through P_3 is very low, and E_3/E_I never reaches 1.0, which it would were it not for the helical coil segment. The value of E_2/E_I fluctuates with a frequency $\Omega = 0.608$. This oscillation occurs because the captured wave travels back and forth across the point P_2 with this frequency.

If the initial straight segment length is less than half the pulse length, reflected waves will return to the struck end before the termination of the pulse application. It was shown in Ref. [8] that under these circumstances, the assembly accepts a large amount of energy. To avoid this, we require

$$ct_0 < 2l, \tag{31}$$

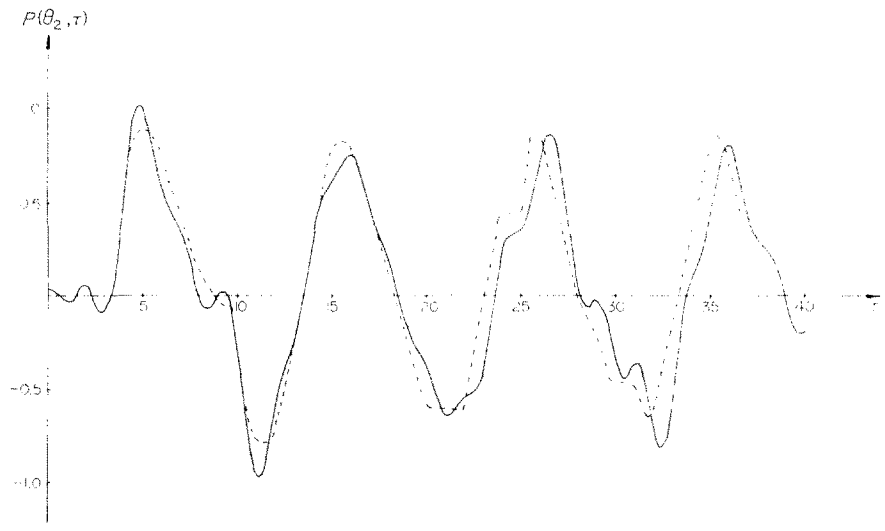

Fig. 5. Tangential stress at point P_2 (dotted line represents experimental results).

where t_0 is the pulse duration and l is the length of the initial straight segment. In Ref. [6] it was shown that pulses shorter than the ring mode period pass readily into the coil, i.e. for effective trapping of the pulse

$$t_0 > 2\pi R/c. \tag{32}$$

Thus, to prevent significant amounts of the shock from reaching the fixed end, the inequalities (31) and (32) must be satisfied.

EXPERIMENTS

The experimental setup is shown in Fig. 2. The helical coil assembly was made of a 1/2-in. diameter aluminum rod. The pulse was generated by dropping a hammer made of the same aluminum rod on top of the assembly. The hammer was guided by a hollow cylinder when falling. The bottom of the assembly was placed tightly in steel block as shown in Fig. 2. By measurement we obtained the following data: diameter of the cross section = 1.26 cm, mean radius of the helical coil = 13.33 cm, length of the top straight segment = 49.5 cm, length of the bottom straight segment = 46.1 cm, bar velocity = 4.952×10^5 cm/sec, length of the hammer = 38.15 cm, the free-falling distance of the hammer = 25.4 cm.

The theory predicts that a rectangular compressive tangential stress pulse of magnitude $(gh/2)^{1/2}/c$ (in strain) and duration $2L/c$ will be generated, where g is the gravitational acceleration, h is the free-falling distance of the hammer, and L is the length of the hammer. Hence, the non-dimensional version of the experimental data is as follows:

$$\begin{aligned} &k = 5.58 \times 10^{-4}, \\ &\theta_2 - \theta_1 = 3.71, \quad \theta_3 - \theta_2 = 2\pi, \quad \theta_4 - \theta_3 = 3.46, \\ &\tau_0 = 5.71. \end{aligned} \tag{33}$$

This was somewhat different from the numerical model of (27), but still comparable.

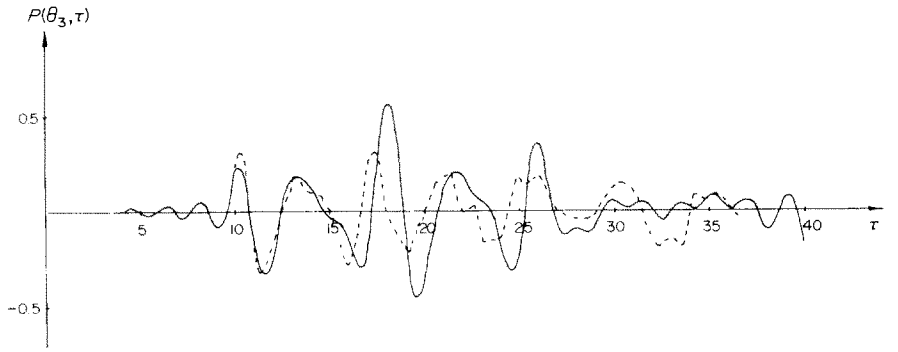

Fig. 6. Tangential stress at point P_3 (dotted line represents experimental results).

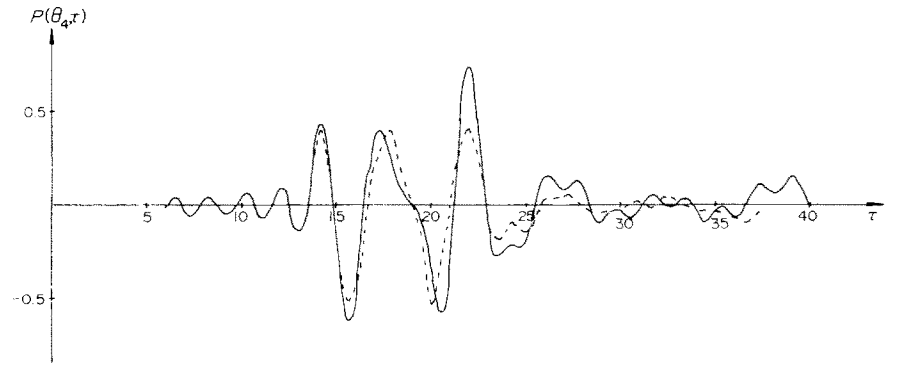

Fig. 7. Tangential stress at point P_4 (dotted line represents experimental results).

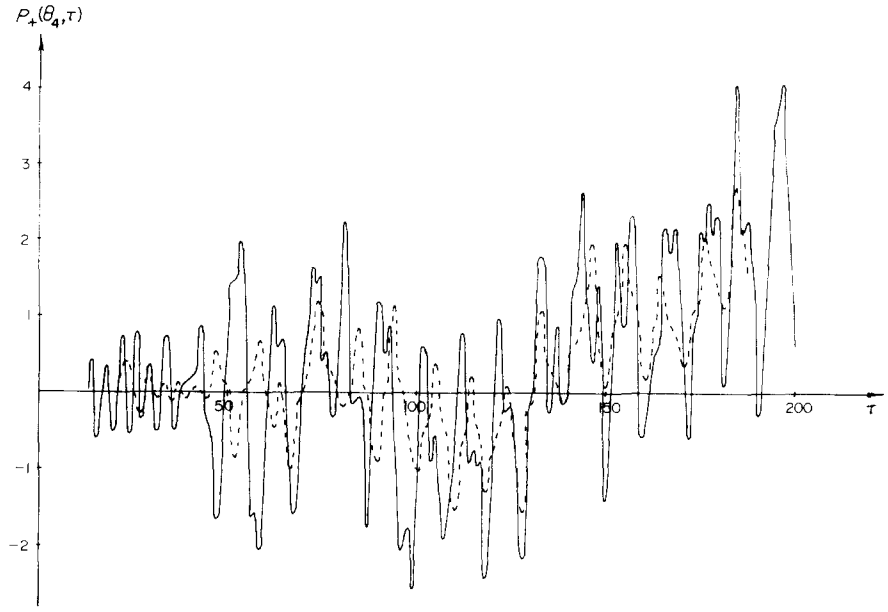

Fig. 8. Outside fiber stress at point P_4 (dotted line represents experimental results).

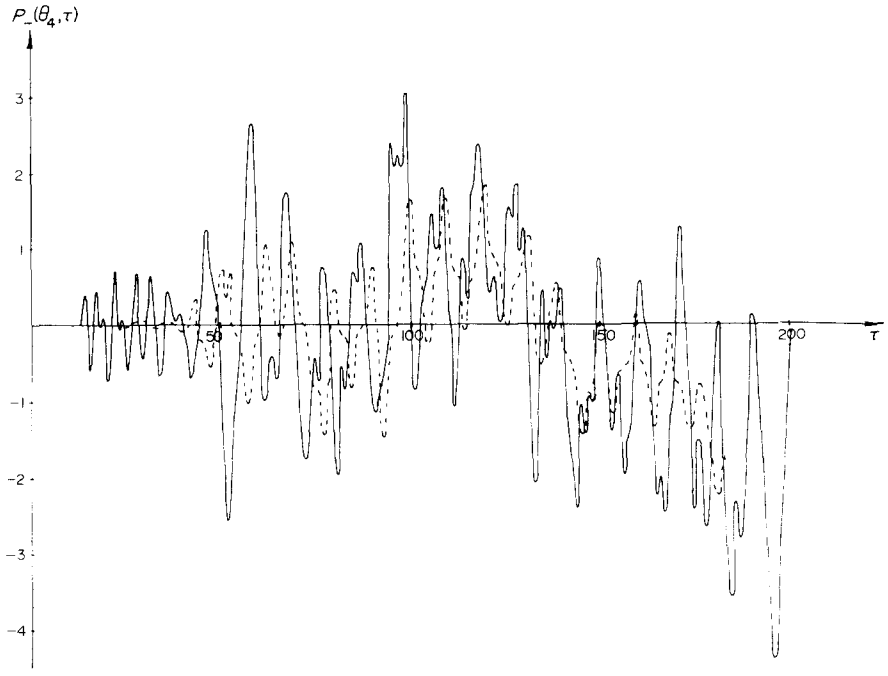

Fig. 9. Inside fiber stress at point P_4 (dotted line represents experimental results).

For strain measurements, BLH Electronics SR-4 type FAE-06N-12S13L strain gages (gage length 1/16-in.) were used. The strain gages were installed at both inside and outside of each of the following locations; mid-point of the top straight segment, points P_2, P_3 and P_4. This arrangement permitted both extensional stress and the bending stress to be measured. The strain was measured by Tektronix type R564B Storage Oscilloscope together with a Tektonix Strain Gage Adapter. The conversion factor for non-dimensionalizing the time is R/c, which was 26.93×10^{-6} sec for this experimental model. Also, the experimentally obtained strain was normalized by the scale factor of $(gh/2)^{1/2}/c$, which in this experiment was 2.25×10^{-4}. The results were plotted in Figs. 4–9 as dotted lines, and the match between the numerical prediction and the experimental result is good. The discrepancy between the two appears to be due to: (1) the differences between the numerical model and the experimental model marked by (27) and (33); (2)

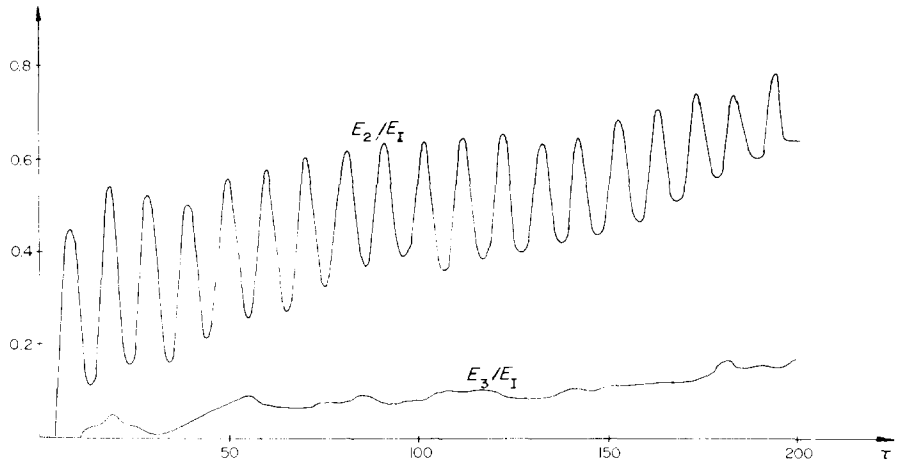

Fig. 10. Energy transmitted beyond points P_2 and P_3.

that the bottom of the assembly was not perfectly rigid in the experiment; and (3) damping in the system which diminished the amplitudes.

CONCLUSIONS

It has been shown that the assembly of Fig. 2 is capable of essentially trapping in its initial straight section the energy from the application of an extensional pulse. However, some flexural energy continuously leaks into the coil portion. In order for the assembly to prevent transmission of shock to the fixed end effectively, the inequalities of (31) and (32) should be satisfied. These criteria may be summarized by requiring the pulse length to be longer than the circumference of the coil but shorter than twice the length of the initial straight segment.

Acknowledgement—This work was supported by the National Science Foundation under grants GK-35913 and ENG74-19873.

REFERENCES

1. W. G. B. Britton and G. O. Langley, Stress pulse dispersion in curved mechanical waveguides. *J. Sound Vib.* **7**, 417 (1968).
2. N. P. Suh, Helical coils as impact load dispersers. *J. Eng. Ind. Trans. ASME* **92**, 197 (1969).
3. D. Y. Hsieh and J. P. Lee, Experimental study of pulse propagation in curved elastic rods. *J. Acoust. Soc. Amer.* **54**, 1052 (1973).
4. J. W. Phillips, Pulse propagation in a helix—theory and experiment. *J. Appl. Mech.* **96**, *Trans. ASME*, **41**, 1047 (1974).
5. D. W. Haines and N. Chang, The helix as a mechanical pulse filter—an example of continuous mechanical systems analyzed by use of the Fourier time transform and the complex frequency response. *Mechanics Res. Com.* **2**, 245 (1975).
6. D. W. Haines and N. Chang, Transmission and reflection of extensional stress pulses at the junction of a straight bar and a helix. *J. Appl. Mech.* To be published.
7. D. W. Haines, Approximate theories for wave propagation and vibrations in elastic rings and helical coils of small pitch. *Int. J. Solids Structures* **10**, 1405 (1974).
8. N. Chang, Helical coil assemblies as mechanical pulse filters—theory and experiment. Ph.D. Thesis, University of South Carolina (1975).
9. F. B. Hildebrand, *Advanced Calculus for Applications*, Chap. 10. Prentice-Hall, Englewood Cliffs, New Jersey (1963).